ARTICLE

Theoretical Study on the High-Temperature $P\bar{6}$ and $P\bar{6}'$ Phases of Si_3N_4: A Tool to Aid in Ceramics Development

Ben-hai Yu, Dong Chen*

College of Physics and Electronic Engineering, Xinyang Normal University, Xinyang 464000, China

(Dated: Received on August 15, 2013; Accepted on October 14, 2013)

Atomistic modeling based on the density functional theory combined with the quasi-harmonic approximation is used to investigate the lattice parameters and elastic moduli of the $P\bar{6}$ and $P\bar{6}'$ phases of Si_3N_4. β-Si_3N_4 is set as a benchmark system since accurate experiments are available. The calculated lattice constants and elastic constants of β-Si_3N_4 are in good agreement with the experimental data. The crystal anisotropy, mechanical stability, and brittle behavior of $P\bar{6}$- and $P\bar{6}'$-Si_3N_4 are also discussed in the pressure range of 30−55 GPa. The results show that these two polymorphs are metallic compounds. The brittleness and elastic anisotropy increase with applied pressure increasing. Besides, the phase boundaries of the $\beta\rightarrow P\bar{6}'\rightarrow\delta$ transitions are also analysed. The β phase is predicted to undergo a phase transition to the $P\bar{6}'$ phase at 40.0 GPa and 300 K. Upon further compression, the $P\bar{6}'\rightarrow\delta$ transition can be observed at 53.2 GPa. The thermal and pressure effects on the heat capacity, cell volume and bulk modulus are also determined. Some interesting features are found at high temperatures.

Key words: First-principles, Nitrides, Brittleness, Phase diagram

I. INTRODUCTION

Silicon nitride (Si_3N_4) belongs to the group-IV nitrides exhibiting unique physical properties. As an important ceramic, Si_3N_4 can be used as gas turbines, cutting tools, etch masks, solar cells, and energy conversion materials [1, 2]. Its low density, high strength, tunable electrical conductivity and high decomposition temperature lead to numerous applications [1, 3]. There are several Si_3N_4 polymorphs, namely α phase (space group: $P3_1c$) [4], β phase (space group: $P6_3/m$) [4], willemite-II phase (wII-Si_3N_4, space group: $I\bar{4}3d$) [5], γ phase (space group: $Fd\bar{3}m$) [6], δ phase (space group: $P3$) [7], and post-spinel phase (space group: BBMM) [8]. In recent years, the $\alpha\rightarrow\beta$ [9, 10], $\beta\rightarrow$wII [5], $\beta\rightarrow\gamma$ [7, 11−13], $\alpha\rightarrow\gamma$ [7], $\beta\rightarrow\delta$ [7], and $\gamma\rightarrow$post-spinel [8, 14] phase transitions have been carefully investigated.

Xu *et al.* found new Si_3N_4 polymorphs (the hexagonal $P\bar{6}$ and $P\bar{6}'$ phases, space group: $P3$), and observed the high-pressure $\beta\rightarrow P\bar{6}'\rightarrow\delta$ phase transitions [7]. Although many efforts have been made on Si_3N_4, the $P\bar{6}$ and $P\bar{6}'$ phases are far less studied than their counterparts α-, β-, wII-, δ- and γ-Si_3N_4. Due to the difficulties in the preparation of polycrystalline samples [7], theoretical calculations, especially first-principles method, can help. Using first-principles calculation, we provide predictions of the thermal quantities, elastic properties, phase stabilities, and phase transition characters of the β, $P\bar{6}$, $P\bar{6}'$, and δ phases.

II. BENCHMARK CALCULATION

Present calculations are performed using the first-principles plane-wave method [15] in combination with ultrasoft pseudo-potentials (US-PP) [16] to calculate the total energy of Si_3N_4. The Perdew-Burke-Ernzerhof functional [17] is used for the exchange-correlation potential. In consideration of accuracy, the plane-wave cut off energies of 500 eV (β-Si_3N_4), 450 eV ($P\bar{6}$-Si_3N_4), 450 eV ($P\bar{6}'$-Si_3N_4), and 450 eV (δ-Si_3N_4) are used in our calculation. The k-point meshes, based on the Monkhorst-Pack scheme [18], are 4×4×12 for β-Si_3N_4, 5×5×12 for $P\bar{6}$-Si_3N_4, 5×5×12 for $P\bar{6}'$-Si_3N_4, and 6×6×15 for δ-Si_3N_4, respectively. The internal coordinates of different atoms have been fully relaxed. Reference configurations for the valence electrons are $Si3s^23p^2$ and $N2s^22p^3$. The calculated total energies of Si_3N_4 are converged to less than 1 μeV/atom. Besides, the crystal structures and atomic coordinates of $P\bar{6}$- and $P\bar{6}'$-Si_3N_4 can be found in Ref.[7].

The k-point mesh should be described in order to avoid the unclearness. In fact, the k-points are determined by the equation $(1/a{:}1/b{:}1/c)$, where a, b, and c are the lattice constants. For β-Si_3N_4, the experimental values of the lattice constants are a=b=0.7607 nm and c=0.2907 nm (see Table I), thus $1/a{:}1/b{:}1/c\approx$1:1:2.62. The k-point mesh can be chosen as 3×3×8, 4×4×12,

*Author to whom correspondence should be addressed. E-mail: chchendong2010@163.com, Tel.: +86-376-6391731, FAX: +86-376-6391731

5×5×14, *etc.* According to our convergence tests, the plane-wave cutoff 500 eV and the k-points 4×4×12 can generate good results for β-Si_3N_4. For the hexagonal $P\bar{6}$- and $P\bar{6}'$-Si_3N_4, we do not know the experimental lattice constants. The only known parameters are the internal coordinates of atoms [7]. We have built the unit cell for $P\bar{6}'$-Si_3N_4 using a=b=1.0 nm and c=0.5 nm. After geometry optimization and full relaxation of internal coordinates with very high cut-off energy and k-points, the equilibrium lattice constants can be obtained. According to the equation ($1/a$:$1/b$:$1/c$) and the convergence tests, the adequate parameters for $P\bar{6}'$- and $P\bar{6}$-Si_3N_4 are found to be cut-off energy of 450 eV and k-points 5×5×12.

Then, we apply the quasi-harmonic approximation (QHA) scheme [19, 20], in which the non-equilibrium Gibbs function $G^*(V;P,T)$ can be determined by

$$G^*(V;P,T) = E(V) + pV + A_{\rm vib}(V;T) \tag{1}$$

where $E(V)$ is the total energy, pV represents the hydrostatic pressure condition, $A_{\rm vib}$ is the vibrational term, which can be written as [21]:

$$A_{\rm vib}(\theta_D;T) = nkT\left\{\frac{9\theta_D}{8T} + 3\ln\left[1 - \exp\left(-\frac{\theta_D}{T}\right)\right] - D\left(-\frac{\theta_D}{T}\right)\right\} \tag{2}$$

where n, θ_D, T, and $D(\theta_D/T)$ are the number of atoms, the Debye temperature, the temperature and the Debye integral, respectively. Accordingly, $G^*(V;P,T)$ can be minimized by

$$\left[\frac{\partial G^*(V;p,T)}{\partial V}\right]_{p,T} = 0 \tag{3}$$

By solving Eq.(3), some thermal properties such as constant-volume heat capacity (C_V), isobaric heat capacity (C_P) and isothermal bulk modulus (B_T) can be obtained by

$$C_V = 3nk_{\rm B}\left[4D\left(\frac{\theta_D}{T}\right) - \frac{3\theta_D/T}{\exp(\theta_D/T)-1}\right] \tag{4}$$

$$C_P = C_V(1+\alpha\gamma T) \tag{5}$$

$$B_T = -\frac{1}{x^2}B_0 e^a(1-x)f(x) \tag{6}$$

$$f(x) = x - 2 - ax(1-x) \tag{7}$$

$$a = \frac{3}{2}(B_0' - 1) \tag{8}$$

$$x = \left(\frac{V}{V_0}\right)^{1/3} \tag{9}$$

$$V = V_0 \exp\left(-\frac{0.85}{0.15B_0'}\right)\cdot \exp\left[-\frac{L^*}{0.15}(p-p_{\rm sp})^{0.15}\right] \tag{10}$$

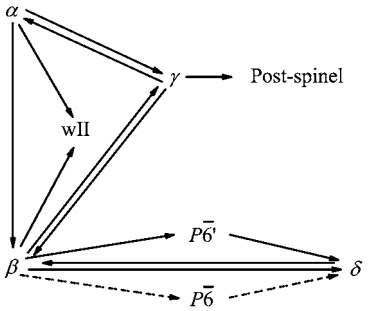

FIG. 1 All-known polymorphs of Si_3N_4 and the transition paths among these phases. The dashed lines denote the $\beta\rightarrow P\bar{6}\rightarrow\delta$ transitions.

TABLE I Lattice constants a, c, and cell volume V of the β, $P\bar{6}'$, $P\bar{6}$, and δ phases.

	a/nm	c/nm	V/Å^3
β-Si_3N_4	0.7632	0.2915	147.0
	0.7593 [22]	0.2921 [22]	145.8
	0.7622 [23]	0.2910 [23]	146.4
	0.7607 [24]	0.2907 [24]	145.7
	0.7607 [25]	0.2911 [25]	145.9
	0.7595 [26]	0.2902 [26]	144.9
	0.7533 [27]	0.2934 [27]	144.2
$P\bar{6}'$-Si_3N_4	0.7062[a]	0.2726[a]	117.8[a]
	0.6879[b]	0.2675[b]	109.7[b]
$P\bar{6}$-Si_3N_4	0.7354[a]	0.2924[a]	132.3[a]
	0.7183[b]	0.2771[b]	123.8[b]
δ-Si_3N_4	0.7633	0.2916	147.1

[a] Calculated at 30 GPa.
[b] Calculated at 55 GPa.

where V_0 is the equilibrium volume, $k_{\rm B}$ the Boltzmann's constant, α the thermal expansion coefficient, B_0 the zero-pressure bulk modulus, γ the Grüneisen parameter, $p_{\rm sp}$ the spinodal pressure, L^* the fitting parameter, and B_0' is the first-order derivative of B_0, respectively. A detailed expression of QHA can be found in Refs. [19, 20].

III. RESULTS AND DISCUSSION

The experimentally confirmed and theoretically hypothesized transition paths of the Si_3N_4 polymorphs are illustrated in Fig.1. The $\beta\rightarrow P\bar{6}\rightarrow\delta$ transitions (dashed line) have not been verified by experiments or theoretical studies. In order to have a deep insight into the fundamental properties of Si_3N_4, we have calculated the pressure dependences of lattice constants, cell volumes, elastic constants, and elastic moduli. The results are shown in Tables I and II.

Since the experimental data of β-Si_3N_4 are available, we have calculated the fundamental properties of the

DOI:10.1063/1674-0068/27/01/103-108

TABLE II Calculated elastic constants C_{ij} (in GPa), bulk modulus $B_{\rm H}$ (in GPa), shear modulus $G_{\rm H}$ (in GPa), Young's modulus $Y_{\rm H}$ (in GPa), Poisson ratio σ and anisotropy factor A of $P\bar{6}$- and $P\bar{6}'$-Si_3N_4.

	P/GPa	C_{11}	C_{12}	C_{13}	C_{33}	C_{44}	$B_{\rm H}$	$G_{\rm H}$	$B_{\rm H}/G_{\rm H}$	$Y_{\rm H}$	σ	A
$P\bar{6}'$-Si_3N_4	30	488.1	300.6	198.9	490.7	160.8	317.1	129.7	2.444	342.4	0.320	1.107
	35	503.5	311.7	211.8	512.6	164.4	331.3	132.5	2.500	350.7	0.323	1.109
	40	520.9	323.8	225.3	534.9	167.1	346.5	135.5	2.557	359.6	0.327	1.104
	45	537.4	335.4	238.2	545.4	169.0	359.5	137.3	2.618	365.3	0.330	1.114
	55	577.1	360.8	268.7	581.5	174.5	391.6	143.4	2.730	383.4	0.336	1.123
$P\bar{6}$-Si_3N_4	30	511.7	262.2	248.4	517.8	98.1	339.9	115.3	2.947	310.7	0.347	0.736
	35	513.5	277.5	271.9	521.6	99.3	354.6	111.3	3.185	302.2	0.357	0.808
	40	514.2	296.3	285.9	534.1	95.8	366.5	105.9	3.460	289.7	0.368	0.804
	45	503.4	311.9	309.5	529.8	89.1	377.5	94.9	3.977	262.6	0.384	0.860
	55	513.1	344.6	332.4	538.5	82.9	398.1	86.8	4.586	242.7	0.399	0.857

β phase. As shown in Table I, the predicted lattice constants and cell volumes are in excellent agreement with the experimental data and the theoretical results. The calculated elastic constants of β-Si_3N_4 given in our previous work [10] were also in satisfactory agreement with the results in Refs.[7, 22]. For $P\bar{6}$- and $P\bar{6}'$-Si_3N_4, a, c, and V decrease with the pressure increasing. The cell volume of the $P\bar{6}$ phase is larger than that of the $P\bar{6}'$ phase. Therefore, the channels in the $P\bar{6}'$ phase are larger than those in $P\bar{6}'$-Si_3N_4.

It is well known that the elastic constants are calculated by means of Taylor expansion of the total energy, $E(V,\delta)$, for the system with respect to a small strain δ of the cell volume V. The energy of a strained system can be expressed as follows [28]:

$$E(V,\delta) = E(V_0,T) + V_0\Big(\sum \tau_i\xi_i\delta_i + \frac{1}{2}\sum C_{ij}\tau_i\xi_i\delta_i\Big) \tag{11}$$

where, $E(V_0,T)$ is the energy of the unstrained system with equilibrium volume V_0 at different temperatures, τ_i is an element in the stress tensor, and ξ_i is a factor to consider Voigt index [28]. The total energy $E(V_0,T)$ at a certain temperature T and the finite temperature lattice constant can be obtained by the vibrational Debye-like model. According to the Voigt-Reuss-Hill approximation, the bulk modulus $B_{\rm H}$, shear modulus $G_{\rm H}$, Young's modulus $Y_{\rm H}$, Poisson ratio σ and anisotropy factor A can be obtained by [29]

$$B_{\rm H} = \frac{1}{2}(B_{\rm V} + B_{\rm R}) \tag{12}$$

$$G_{\rm H} = \frac{1}{2}(G_{\rm V} + G_{\rm R}) \tag{13}$$

$$Y_{\rm H} = \frac{9B_{\rm H}G_{\rm H}}{3B_{\rm H} + G_{\rm H}} \tag{14}$$

$$\sigma = \frac{1}{2}\frac{3B_{\rm H} - 2G_{\rm H}}{3B_{\rm H} + G_{\rm H}} \tag{15}$$

$$A = \frac{4C_{44}}{C_{11} + C_{33} - 2C_{13}} \tag{16}$$

where the subscripts V, R, and H are the Voigt index, the Reuss index, and the Hill index, respectively. These quantities are listed in Table II.

For a hexagonal lattice, there are five independent elastic constants C_{11}, C_{12}, C_{13}, C_{33}, and C_{44} ($2C_{66}$=$C_{11}-C_{12}$). As listed in Table II, the elastic constants C_{ij}, elastic moduli $B_{\rm H}$, $G_{\rm H}$, and $Y_{\rm H}$ of $P\bar{6}'$-Si_3N_4 increase monotonously with applied pressure, but the slopes are different. The pressure effect on C_{ij} is significant. The decrease of C_{44} reflects the shear resistance decreases in the {010} or {100} plane in the ⟨001⟩ direction. The value of the Poisson ratio σ for covalent materials is quite small (about 0.1), whereas for metallic materials a typical σ is 0.33 [30]. The calculated σ is 0.320−0.336, showing moderate lateral expansion when compressed. The $P\bar{6}'$ phase is a metallic compound in the whole pressure range of 30−55 GPa. The anisotropy factor A=1 represents completely elastic isotropy while any value smaller or larger than 1 indicates elastic anisotropy. A increases as the pressure increases first, then the elastic anisotropy of $P\bar{6}'$-Si_3N_4 is quite small at 40 GPa. When P>40 GPa, A will gradually strengthen with the pressure increasing. Besides, the $B_{\rm H}/G_{\rm H}$ ratio reflects the brittle and ductile behaviors of polycrystalline materials since solids behave in brittle manners if $B_{\rm H}/G_{\rm H}$>2 [31]. $P\bar{6}'$-Si_3N_4 remains brittle in the pressure range of 30−55 GPa. The brittleness increases with the pressure increasing. More importantly, the chemical bonds in $P\bar{6}'$-Si_3N_4 are ionic due to the fact that the typical B/G ratios for covalent and ionic solids are 0.91 and 1.67, respectively.

In Table II, we can see that the elastic moduli of $P\bar{6}$-Si_3N_4 do not follow the same trend. C_{12}, C_{13}, and $B_{\rm H}$ increase with the increasing pressure whereas $G_{\rm H}$ and $Y_{\rm H}$ show the opposite trends. C_{11}, C_{33}, and C_{44} increase first, and then decrease with the increasing pressure. The calculated σ is 0.347−0.399, which indicates that $P\bar{6}$-Si_3N_4 is a metallic compound. The variation of A with pressure ($P\bar{6}$-Si_3N_4) is similar to that

DOI:10.1063/1674-0068/27/01/103-108

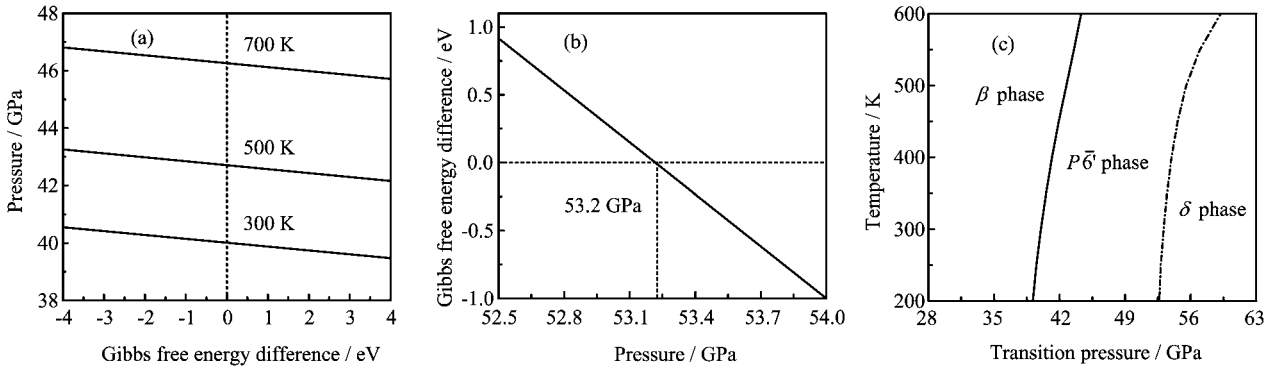

FIG. 2 (a) Gibbs free energy difference ($G_{P\bar{6}'}-G_{\beta}$) as a function of pressure. (b) Critical pressure as a function of Gibbs free energy difference of the $P\bar{6}'\rightarrow\delta$ transition at 300 K. (c) Relationships of the transition pressures of the $\beta\rightarrow P\bar{6}'\rightarrow\delta$ transitions with temperature.

of $P\bar{6}$-Si_3N_4. The anisotropy of $P\bar{6}$-Si_3N_4 is stronger than that of $P\bar{6}'$-Si_3N_4 since $|A(P\bar{6}')-1|>|1-A(P\bar{6})|$. According to the B_H/G_H ratio, $P\bar{6}$-Si_3N_4 is more brittle than $P\bar{6}'$-Si_3N_4. For a hexagonal structure, the mechanical stability can be determined by the Born's criteria [32]: $C_{11}-|C_{12}|>0$, $C_{44}>0$, $(C_{11}+C_{12})C_{33}-2C_{13}^2>0$. At 0 K, $P\bar{6}$- and $P\bar{6}'$-Si_3N_4 are stable in the pressure range of 30−55 GPa since all the elastic constants satisfy these criteria. Besides, the bulk moduli of the two phases are greater than the bulk moduli of α, β, and γ phases [33].

The transition pressures among different phases of solids can be obtained by comparing the Gibbs free energy G of different phases. We have calculated the Gibbs free energy difference between β-Si_3N_4 and $P\bar{6}'$-Si_3N_4, as shown in Fig.2(a). The thermodynamic requirement, for the equality of G, at the critical points, suggests that the transition pressures of the $\beta\rightarrow P\bar{6}'$ transition are 40.0, 42.7, and 46.2 GPa at temperatures of 300, 500, and 700 K, respectively. β-Si_3N_4 has the lower free energy at low pressures, which indicates that this phase is the low-temperature phase of Si_3N_4. The Gibbs free energy difference obtained, $G_{\delta}-G_{P\bar{6}'}$, as a function of pressure is given in Fig.2(b). It is clearly seen that the transition pressure between the $P\bar{6}'$ phase and the δ phase is 53.2 GPa (at 300 K), at which the $P\bar{6}'$ phase will automatically transform into δ-Si_3N_4. $P\bar{6}'$-Si_3N_4 has the lower free energies when $P<53.2$ GPa. The δ phase has the lower free energies at higher pressure, *i.e.* δ-Si_3N_4 would be favored at sufficiently high pressures. The δ phase boundaries of the $\beta\rightarrow P\bar{6}'\rightarrow\delta$ transitions are illustrated in Fig.2(c).

As shown in Fig.2(c), the slopes of the $\beta\rightarrow P\bar{6}'$ and $P\bar{6}'\rightarrow\delta$ transitions are both positive, which suggests that at higher temperatures it will require higher pressures to synthesize $P\bar{6}'$-Si_3N_4/δ-Si_3N_4. It is found that the transition pressure from the β phase to the $P\bar{6}'$ phase is 40.0 GPa (at 300 K). The critical pressure of the $\beta\rightarrow P\bar{6}'$ transition is about 13 GPa higher than that of the $P\bar{6}'\rightarrow\delta$ transition. According to the Clausius-Clapeyron relation [11], the slope of the phase boundary can be determined by $\Delta S/\Delta V$, where ΔS and ΔV are the entropy change and the volume variation, respectively. Therefore, the $\beta\rightarrow P\bar{6}'\rightarrow\delta$ transitions are accompanied by the shrinkage of volume, which is in agreement with the cell volumes listed in Table I (the calculated volume of δ-Si_3N_4 at 55 GPa is 109.6 Å^3).

One of the most important vibrational properties of solids is the temperature dependence of heat capacity. Figure 3 (a) and (b) give the evolutions of the constant-pressure heat capacity C_P with temperature for $P\bar{6}$- and $P\bar{6}'$-Si_3N_4, respectively. As shown in Fig.3(a), C_P is very small at low temperature. From 0 to 500 K, C_P increases exponentially with the temperature increasing. At high temperatures, C_P follows a linear increase, which is not similar to the constant-volume heat capacity C_V (C_V follows the Dulong-Petit's law, *i.e.* 3R for monoatomic solids). Although C_V gives direct information on the intrinsic anharmonic effects, it is C_P that is experimentally measured, and it contains both anharmonic effects and quasi-harmonic contributions. In Fig.3(b), it is clearly seen that C_P increases rapidly at low temperatures, and reaches a plateau region at high temperatures. The heat capacity of $P\bar{6}$-Si_3N_4 is larger than that of $P\bar{6}'$-Si_3N_4 at the same temperature.

In Fig.3(c), it is clearly seen that the volumes of $P\bar{6}$- and $P\bar{6}'$-Si_3N_4 decrease smoothly as pressure increases. The V/V_0 ratio of $P\bar{6}$-Si_3N_4 decreases faster than that of $P\bar{6}'$-Si_3N_4. At high pressures, the difference between the two curves can be clearly seen. This means that the $P\bar{6}$ phase is more compressible than the $P\bar{6}'$ phase. Figure 3(d) shows the evolutions of bulk moduli with pressure at 300 K. The bulk modulus increases with the increasing pressure but the rate of increase is moderate. The first sticking feature is that the bulk modulus of $P\bar{6}'$-Si_3N_4 is greater than that of $P\bar{6}$-Si_3N_4. The second feature is that the slopes of the two curves are different. At 50 GPa and 300 K, the calculated bulk modulus and heat capacity are 391.4 GPa (343.2 GPa) and 44.8 J/(mol K) (77.2 J/(mol K)) for

DOI:10.1063/1674-0068/27/01/103-108

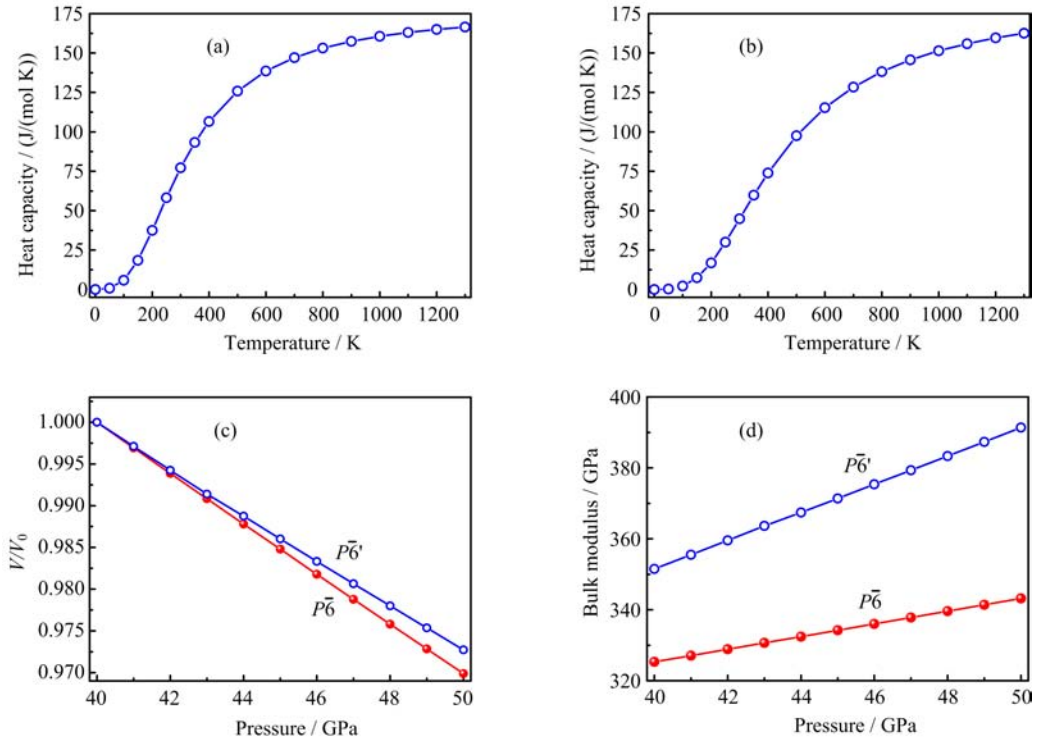

FIG. 3 The constant-pressure heat capacity C_P (at 50 GPa) for (a) $P\bar{6}$-Si_3N_4, (b) $P\bar{6}'$-Si_3N_4, (c) the normalized cell volume V/V_0 (V_0 is the equilibrium cell volume at 40 GPa), and (d) bulk modulus of Si_3N_4 at 300 K.

$P\bar{6}'$-Si_3N_4 ($P\bar{6}$-Si_3N_4), respectively.

IV. CONCLUSION

First-principles calculations are carried out on Si_3N_4 in the recently-discovered $P\bar{6}'$ and $P\bar{6}$ phases to investigate their stability and physical properties, which have not yet been established experimentally. As a benchmark system (β-Si_3N_4), the calculated lattice constants and elastic moduli are in agreement with the experimental data. The lattice parameters, cell volume, elastic constants, elastic moduli, anisotropy factor and Poisson ratio of $P\bar{6}$- and $P\bar{6}'$-Si_3N_4 are also predicted in the pressure range of 30−55 GPa. β-Si_3N_4 is predicted to undergo a first-order phase transition to the $P\bar{6}'$ phase at 40.0 GPa and 300 K. Upon further compression, the $P\bar{6}'\rightarrow\delta$ transformation can be observed at 53.2 GPa. The positive slopes of the $\beta\rightarrow P\bar{6}'\rightarrow\delta$ transitions mean that the two phase transformations are accompanied by the shrinkage of volume. The two polymorphs are brittle compounds with little metallic character, which is not similar to the β phase. The anisotropy of $P\bar{6}'$-Si_3N_4 increases with the increasing pressure while the anisotropy of $P\bar{6}$-Si_3N_4 shows the opposite trend. The heat capacity increases rapidly at low pressures, and reaches a plateau at high pressures. Furthermore, the $P\bar{6}$ phase is more compressible than the $P\bar{6}'$ phase.

V. ACKNOWLEDGMENTS

This work was supported by the National Natural Science Foundation of China (No.U1204501, No.11105115, and No.11304141), the Project of Basic and Advanced Technology of Henan Province of China (No.112300410021), and the Key Project of Henan Educational Committee (No.12A140010). The authors are grateful to Prof. M. A. Blanco from the Departamento de Química Físicay Analitica, Faculatad de Química, Universidad de Oviedo for the Gibbs code.

[1] S. Y. Ren and W. Y. Ching, Phys. Rev. B **23**, 5454 (1981).
[2] W. X. Wang, D. H. Li, Z. C. Liu, and S. H. Liu, Appl. Phys. Lett. **62**, 321 (1993).
[3] Y. N. Xu and W. Y. Ching, Phys. Rev. B **51**, 17379 (1995).
[4] S. D. Mo, L. Z. Ouyang, W. Y. Ching, I. Tanaka, Y. Koyam, and R. Riedel, Phys. Rev. Lett. **83**, 5046 (1999).
[5] P. Kroll, J. Solid State Chem. **176**, 530 (2003).
[6] A. Zerr, G. Miehe, G. Serghiou, M. Schwarz, E. Kroke, R. Riedel, H. Fueß, P. Kroll, and R. Boehler, Nature (London) **400**, 340 (1999).
[7] B. Xu, J. J. Dong, P. F. McMillan, O. Shebanova, and A. Salamat, Phys. Rev. B **84**, 014113 (2011).

DOI:10.1063/1674-0068/27/01/103-108

[8] K. Tatsumi, I. Tanaka, and H. Adachi, J. Am. Ceram. Soc. **85**, 7 (2002).
[9] N. V. Danilenko, G. S. Oleinik, V. D. Dobrovol'skii, V. F. Britun, and N. P. Semenenko, Sov. Powder Metal. Met. Ceram. **31**, 1035 (1992).
[10] B. H. Yu and D. Chen, Chin. Phys. B **21**, 060508 (2012).
[11] A. Kuwabara, K. Matsunaga, and I. Tanaka, Phys. Rev. B **78**, 064104 (2008).
[12] A. Togo and P. Kroll, J. Comput. Chem. **29**, 2255 (2008).
[13] H. L. He, T. Sekine, T. Kobayashi, and H. Hirosaki, Phys. Rev. B **62**, 11412 (2000).
[14] P. Kroll and J. von Appen, Phys. Stat. Sol. B **226**, R6 (2001).
[15] P. Hohenberg and W. Kohn, Phys. Rev. **136**, B864 (1964).
[16] D. Vanderbilt, Phys. Rev. B **41**, 7892 (1990).
[17] J. P. Perdew, K. Burke, and M. Ernzerhof, Phys. Rev. Lett. **77**, 3865 (1996).
[18] H. J. Monkhorst and J. D. Pack, Phys. Rev. B **13**, 5188 (1976).
[19] M. A. Blanco, E. Francisco, and V. Luaña, Comput. Phys. Commun. **158**, 57 (2004).
[20] A. Otero-de-la-Roza and V. Luaña, Comput. Phys. Commun. **182**, 1708 (2011).
[21] M. Flórez, J. M. Recio, E. Francisco, M. A. Blanco, and A. Martin Pendás, Phys. Rev. B **66**, 144112 (2002).
[22] C. M. Marian, M. Gastreich, and J. D. Gale, Phys. Rev. B **62**, 3117 (2000).
[23] W. Y. Ching, L. Z. Ouyang, and J. D. Gale, Phys. Rev. B **61**, 8696 (2000).
[24] M. Yashima, Y. Ando, and Y. Tabira, J. Phys. Chem. B **111**, 3609 (2007).
[25] H. F. Priest, F. C. Burns, G. L. Priest, and E. C. Skaar, J. Am. Ceram. Soc. **56**, 395 (1973).
[26] N. Hirosaki, S. Ogata, C. Kocer, H. Kitagawa, and Y. Nakamura, Phys. Rev. B **65**, 134110 (2002).
[27] W. Y. Ching, Y. N. Xu, J. L. D. Gale, and M. Rühle, J. Am. Ceram. Soc. **81**, 3189 (1998).
[28] L. Fast, J. M. Wills, B. Johansson, and O. Eriksson, Phys. Rev. B **51**, 17431 (1995).
[29] M. B. Kanoun, S. Goumri-Said, A. H. Reshak, and A. E. Merad, Solid State Sci. **12**, 887 (2010).
[30] J. Haines, J. M. Leger, and G. Bocquillon, Annu. Rev. Mater. Res. **31**, 1 (2001).
[31] S. F. Pugh, Philos. Mag. Ser. **45**, 823 (1954).
[32] M. Born and K. Huang, *Dynamical Theory of Crystal Lattics*, Oxford: Clarendon, (1956).
[33] C. Zhang, J. X. Sun, R. G. Tian, and S. Y. Zou, Acta Phys. Sin. **56**, 5969 (2007).

DOI:10.1063/1674-0068/27/01/103-108